Contents lists available at ScienceDirect

Heliyon

journal homepage: www.cell.com/heliyon

Research article

Multifunctional properties of spherical silver nanoparticles fabricated by different microbial taxa

Sultan M. Alsharif [a], Salem S. Salem [b], Mohamed Ali Abdel-Rahman [b], Amr Fouda [b, *],
Ahmed Mohamed Eid [b], Saad El-Din Hassan [b], Mohamed A. Awad [c], Asem A. Mohamed [d]

[a] Biology Department, Faculty of Science, Taibah University, Al Madinah, KSA
[b] Botany and Microbiology Department, Faculty of Science, Al-Azhar University, 11884, Nasr City, Cairo, Egypt
[c] Department of Zoology and Entomology, Faculty of Science, Al-Azhar University, 11884, Nasr City, Cairo, Egypt
[d] National Research Centre, El-Behouth St., Dokki, P.O. 12622, Giza, Egypt

ABSTRACT

This study addresses the impacts of metabolites from different microbial taxa on the fabrication and multifunctional biological properties of spherical silver nanoparticles (Ag-NPs). Three microbial taxa, a bacterial (*Bacillus cereus* A1-5), actinomycetes (*Streptomyces noursei* H1-1), and fungal (*Rhizopus stolonifer* A6-2) strains were used for Ag-NPs biosynthesis, whereas *Streptomyces noursei* is demonstrated for the first time. These isolates were identified using either 16S rRNA or ITS gene sequencing. Characterization of Ag-NPs was done using color change analysis, Uv-Vis spectroscopy, FT-IR spectroscopy, XRD, TEM, SEM-EDX, DLS, and Zeta potential analysis. All biosynthesized NPs exhibited spherical shape with different sizes ranged from 6–50 nm, 6–30 nm and 6–40 nm for NPs obtained by A1-5, H1-1 and A6-2, respectively. The crystalline center cubic face of Ag-NPs was confirmed using XRD at 2θ values 38.08$^{\rm o}$, 44.27$^{\rm o}$, 64.41$^{\rm o}$ and 77.36$^{\rm o}$. FT-IR analysis revealed varied intense absorption peaks for biomolecules required for NPs synthesize by each microbial strain. The stability of spherical Ag-NPs was confirmed due to highly DLS negative surface charge of −17.5mV, −18.9mV, and −15.6mV for NPs synthesized by strains A1-5, H1-1, and A6-2, respectively. Ag-NPs exhibited a broadspectrum of antibacterial activity against Gram-positive and Gram-negative bacteria with varied effectiveness. They also exhibited a cytotoxic effect against cancer cell line (caco-2) in a dose-dependent pattern with IC50 of 8.9 ± 0.5, 5.6 ± 3.0, 11.2 ± 0.5 μg/ml for NPs synthesized by strains A1-5, H1-1, and A6-2, respectively. Moreover, these spherical Ag-NPs showed larvicidal activity against the 3$^{\rm rd}$ instar larvae of the dengue vector *Aedes aegypti*.

1. Introduction

Nanotechnology is the production or manufacturing of nanoscale materials (1–100 nm), while nano-biotechnology is the integration between biology and nanotechnology to construct new nanomaterials for biotechnological applications. Nanomaterials with specific shapes can be synthesized by various methods including physical, chemical, or biological methods. However, chemical and physical methods are highly expensive, requiring toxic chemical and high energy consumption (Al-Shmgani et al., 2017). Besides this, the synthesized particles are not of expected purity whereas their surfaces were found to be sediment with chemicals. Additionally, preparation of specific Ag-NPs size is highly difficult and require a further processing step to prevent particle aggregation (Malik et al., 2002). Therefore, recent attention is drawn to

green syntheses of nanomaterials because of its safety, eco-friendly, cost-effective, and easily scaled up (Luo et al., 2018; Salem and Fouda, 2020). The synthesis of particular shapes and sized of nanoparticles (NPs) specially nano-silver (Ag-NPs) through green approach are paid more attention because their frequent use in various fields such as magnetic devices, historical paper conservation against deteriorated fungi, photocatalysis, microelectronics, anticorrosive coatings, biomedicals, anti-inflammatory, antibacterial, drug delivery, bioactivity, bioavailability, tumor targeting and bio-absorption (Fouda et al., 2019a, 2019b; Hassan et al., 2019; Shaheen and Fouda, 2018; Shaheen et al., 2019; Sharaf et al., 2019).

The huge applications of Ag-NPs are attributed to unique physical and chemical properties including electrical, optical, thermal stability, a wide range of surface plasmon resonance, photoelectrochemical properties,

---

good conductivity and biological properties (Gupta et al., 2017; Rasheed et al., 2017). The synthesis of NPs *via* green approach is an example for a bottom-up method where NPs were formed due to the oxidation/reduction process of metallic ions by secreted biomolecules such as enzymes, proteins, and sugars (Fouda et al., 2017; Mohmed et al., 2017). Recently, different microbial taxa including actinomycetes such as *Streptomyces* spp. (Fouda et al., 2019c), fungi such as *Penicillium italicum* (Taha et al., 2019) and *Fusarium keratoplasticum* A1-3 (Mohamed et al., 2017), and bacterial species such as *Bacillus* sp. SBT8 (Yurtluk et al., 2018) were used for biosynthesis of Ag-NPs by extracellular metabolites. Besides, several metals and metal oxides NPs (e.g. silver, gold, silver-gold alloy, platinum, copper, zinc, selenium, palladium, silica, titanium, magnetite, nickel oxide) are synthesized through either extra or intracellular metabolites of actinomycetes, bacteria, fungi, algae or natural extracts as an effective chelating agents for the formation of nanoscaled particles (Fouda et al., 2018; Hassan et al., 2018; Mohamed et al., 2019; Thomas et al., 2019; Venugopal et al., 2017).

Biosynthesis of Ag-NPs have been reported to exert multifunctional activities with promising therapeutic efficacy to control pathogenic microbes (Soliman et al., 2020; Mukherjee et al., 2014). Also, cytotoxicity and anticancer activities of Ag-NPs were evaluated against breast cancer MCF-7 cell line (Vizhi et al., 2016), HT-29 cell lines (Devi and Bhimba, 2012), Hep2 cell line (Kumar et al., 2016) and Human cervical cancer cell (Yuan et al., 2018), MCF-7 and A549 as breast and lung cancer cells, respectively (Venugopal et al., 2017).

Biosynthesized Ag-NPs are considered cost-effective, eco-friendly, safe and alternative tools for biological control. *Aedes aegypti* is the main vector of dengue fever worldwide and affecting the lives of huge numbers of people every year (Organization, 2016). Medicines and vaccines are not available to prevent or treat these pathogens, therefore, vector control should be a successful approach to reducing disease transmission (Morejón et al., 2018; Salem et al., 2020). The main challenges are to develop a safe larvicidal compound to control *Aedes aegypti* populations.

In this study, the effects of biomass filtrates from different microbial taxa (*Bacillus cereus, Streptomyces noursei,* and *Rhizopus stolonifera*) were separately evaluated and compared for green synthesis of spherical Ag-NPs. The characterization of biosynthesized spherical Ag-NPs was done by Uv-Vis spectroscopy, Fourier transform infra-red (FT-IR) spectroscopy, X-Ray diffraction (XRD) patterns, transmission electron microscopy TEM and Scanning electron microscopy which connected with energy dispersive X-ray (SEM-EDX), Dynamic light scattering (DLS) and Zeta potential analysis. Besides, the multifunctional activities of green synthesized NPs including antibacterial activities against different pathogenic Gram-positive and Gram-negative bacteria, *in-vitro* cytotoxicity against cancer and normal cell line (Caco-2 and Vero cell line respectively) and insecticidal activity against vector-borne dengue fever, *Aedes aegypti* were evaluated.

2. Materials and methods

2.1. Microbial isolation and identification

Bacterial, fungal and actinomycetes strains were isolated from cultivated soil samples (GPS, N: 28 21 14.8 E: 28 51 47.7) collected from Giza governorate, Egypt. The isolation process was conducted using nutrient agar, malt extract agar, and starch nitrate agar media for bacterial, fungal and actinomyceteal strains, respectively (Fouda et al., 2015).

The molecular identification was carried out based on 16S rRNA gene sequencing for bacteria and actinomycetes, or internal transcribed spacer (ITS) region for fungi.

For 16S rRNA: bacterial and actinomycetal genomic DNA were extracted following the modified method by Miller et al. (1999). Briefly, single colonies were picked up from agar plates and suspended in 50 μl sterile deionized H_2O. The cell suspension was then incubated for 10 min in a water bath at 97 °C, followed by centrifugation for 10 min at 15,000 *xg*, then, cell lysate containing DNA was separated. 16S rRNA gene was

amplified with PCR using genomic DNA template and two universal primers. The used primers are as follows: 27f (5-AGAGTTT-GATCCTGGCTCAG-3) and 1492r (5-GGTTACCTTGTTACGACTT-3) (Lane, 1991). The PCR mixture [50 μL] contained 1*x* PCR buffer, 0.5 mM $MgCl_2$, 2.5 U Taq polymerase (QIAGEN), 0.25 mM dNTP, 0.5 μM of each primer, and 1 μl of extracted genomic DNA.

For ITS sequencing: Fungal Genomic DNA was extracted using Gene Jet Plant genomic DNA purification Kit (Thermo). The ITS region was amplified in PCR using the DNA template and two primers of ITS1 (5 -TCCGTAGGTGAACCTGCGG-3) and ITS4 (5 -TCCTCCGCTTATTGA-TATGC-3) (Salem et al., 2019). The PCR mixture (50 μL) contained: Maxima Hot Start PCR Master Mix (Thermo), 0.5 μM of each primer, and 1 μL of extracted DNA.

PCR was performed in a Thermal Cycler by Sigma Scientific Services Company (Cairo, Egypt) with a 3 min hot starting performed at 94 °C, 30 cycles at 94 °C for 30 s, 55 °C for 30 s, and 72 °C for 1 min, followed by gene extension for 10 min at 72 °C. Sequencing was analyzed using ABI 3730x1 DNA sequencer at GATC Company (Germany). The obtained sequences were compared with that on GenBank database using the NCBI BLAST program. The phylogenetic tree was conducted by bootstrap analysis.

2.2. Silver nanoparticles biosynthesis

Extracellular metabolites of the microbial strains were separately used as reducing agents for Ag-NPs biosynthesis using $AgNO_3$ (Sigma Aldrich) as a precursor. Briefly, the bacterial, fungal and actinomycetal strains were inoculated in nutrient broth, malt extract broth and starch nitrate-broth media, respectively at 35 ± 2^oC (for bacteria) or 30 ± 2^oC (for fungi and actinomycetes) and 150 *rpm* shaking conditions for 120h. At the end of incubation period, microbial biomasses were harvested and washed with distilled H_2O to exclude the remaining media components. After that, 10 g of each microbial biomass was separately mixed with 100 mL distilled H_2O for 72 h at 30 ± 2 °C. The mixtures were filtered using Whatman filter paper No.1 to collect biomass filtrate which was used as a starter for Ag-NPs biosynthesis as following: 1mM $AgNO_3$ was then suspended in 100 mL biomass filtrate and incubated at 30 ± 2 °C and 150 *rpm* in dark condition for 24 h. Negative control which represented as biomass filtrate without $AgNO_3$ was run with an experiment.

2.3. Characterizations of Ag-NPs

2.3.1. Ultraviolet-visible (Uv-Vis) spectroscopy

Color changes of the colloidal solution after adding $AgNO_3$ were the first indicator for Ag-NPs synthesis. The maximum surface plasmon resonance (SPR) was detected by measuring the absorbance of the colloidal solution using JANEWAY 6305 Spectrophotometer at wavelength spectral range of 300–600 nm.

2.3.2. Fourier transform infra-red (FT-IR) spectroscopy

The FT-IR analysis was performed for biomass filtrate of microbial strains and biosynthesized Ag-NPs for detection of the functional groups responsible for reducing, stabilizing and capping of NPs. The spectra were measured on the Agilent system Cary630 FTIR model over a range of 4000–400 cm^{-1}.

2.3.3. X-ray diffraction (XRD)

The X-ray pattern of Ag-NPs was analyzed using X-ray diffractometer X'Pert Pro (Philips, Eindhoven, Netherlands). The 2θ range was from 4° to 80°. Ni-filtered Cu Ka radiation was used as source for the X-ray with Voltage of 40 kV and current of 30 mA. The average size of Ag-NPs synthesized by different microbes was calculated using the following Scherrer equation as follows:

$$D = K\lambda / \beta \cos\theta \tag{1}$$

where; K, is the shape constant; λ, is the wavelength of the X-ray; β, is the half-width of the peak and; θ, is the half of the Bragg's angle.

2.3.4. Transmission electron microscopy (TEM)

The size and morphological examinations of biosynthesized silver NPs were achieved by TEM on a JEM-1230 (JEOL, Japan) device with 120 kV acceleration voltage. For the TEM measurements, a colloidal solution containing biosynthesized Ag-NPs was dropped on a copper grid with coated-carbon.

2.3.5. Energy dispersive spectroscopic analysis (SEM-EDX)

The elemental composition of the green synthesized silver-NPs was investigated using SEM (type: JEOL, JSM-6360LA, Japan) which connected with energy dispersive spectroscopy (EDX) instrument.

2.3.6. Dynamic light scattering (DLS)

The distribution of Ag-NPs and their sizes in colloidal solutions were examined by DLS. The sample was re-suspended in distilled water and subjected to DLS measurement using Zeta sizer nano-series (Nano ZS), Malvern, UK. Also, Ag-NPs stability was evaluated by zeta potential measurement.

2.4. Multifunctional properties of Ag-NPs

2.4.1. Antibacterial activity

The antibacterial activity of biosynthesized Ag-NPs obtained by different microbial strains was evaluated using agar-well diffusion method against Gram-positive (*Bacillus subtilis* ATCC6633 and *Staphylococcus aureus* ATCC6538) and Gram-negative (*Salmonella typhimurium* ATCC14028, *Pseudomonas aeruginosa* ATCC9022, and *Escherichia coli* ATCC8739) bacteria. Pure bacterial cultures were prepared and inoculated under aseptic condition using sterilized cotton swap over Muller Hinton ager media. After that, about 100 μL of Ag-NPs solution (100 ppm) was introduced into well (0.7 mm) on Muller-Hinton agar plates. Different Ag-NPs concentrations (75.0 ppm, 50.0 ppm, 25.0 ppm, 15.0 ppm, and 10.0 ppm) were prepared to select a minimal inhibitory concentration (MIC) for each tested organism. The plates were then incubated for 24 h at 35 ± 2 °C. The results were recorded as the diameter of inhibition zones (mm) around each well (Valgas et al., 2007). The experiment was done in triplicate.

2.4.2. In-vitro cell viability of Ag-NPs

2.4.2.1. Cell culture. Two selected cell lines [human colorectal adenocarcinoma cells (Caco-2) as cancer cell and normal Vero cells (kidney of African green monkey)] were obtained from VACSERA Holding Company for Biological Products&Vaccines, Giza, Egypt.

2.4.2.2. MTT assay. The toxicity of biosynthesized Ag-NPs and AgNO$_3$ as control were assessed with cell-viability assay MTT [3-(4, 5-dimethylthiazol-2-yl)-2, 5-diphenyl tetrazolium bromide]. In brief, the cell (1×10^5 cells/mL) grown in 96-well plates and treated with Ag-NPs at different concentrations (double-fold dilution) ranged from 3.9–1000 μg/mL and incubated at 37 °C for 48 h. Further incubation with MTT (5 mg/mL in phosphate-buffered saline) at 37 °C/5% CO$_2$ for 1–5 h was done before addition of the formazan (MTT metabolic product dissolved in 200 μL DMSO) to 96-well plate. The color intensities were measured with an enzyme-linked immunosorbent assay (ELISA) reader at 560 nm (Philip and Kundu, 2003). All performed experiments were conducted in triplicates. The cell viability percentage was then calculated based on control (cells incubated without silver nanoparticles) as follows:

$$\text{Cell viability } \% = \frac{\text{sample absorbance}}{\text{control absorbance}} \times 100 \tag{2}$$

2.4.3. Larvicidal bioassay

2.4.3.1. Larvae rearing. The insecticidal activities of biosynthesized Ag-NPs using different microbes were assessed on *Aedes aegypti* which collected from Medical Entomology Institute, Dokii, Giza, Egypt. The larvae were kept in plastic cups containing dechlorinated tap water and fed on small bread pieces. The experiment was done at 27 ± 2 °C, 75–85 % relative humidity and photoperiod 14:10 light: dark. The bioassay was assessed according to WHO (Organization, 1996) with some modifications. The experiment was conducted in triplicate and each replicate containing 25 larvae. The mortality percent due to 5.0, 10.0, 15.0, 20.0, 25.0, 50.0, 75.0 and 100.0 ppm of Ag-NPs was monitored after larval and pupal stage. The mortality was calculated using the following Abbott's formula (Abbott, 1925):

$$\text{Larval mortality } (\%) = \frac{(\text{Mortality in test concentration} - \text{Mortality in control})}{100 - \text{Mortality in control}} \times 100 \tag{3}$$

2.5. Statistical analysis

All results shown in this study are mean values of three independent replicates. The data were subjected to analysis of variance (ANOVA) using statistical package SPSS v17. The comparison between treatments was analyzed using Tukey HSD test at a significant level of $P \leq 0.05$.

3. Results and discussion

3.1. Identification of microbial strains

The three microbial taxa encoded A1-5, H1-1, and A6-2 were subjected to molecular identification using 16S rRNA gene sequencing for the bacterial and actinomycetal isolates and ITS gene sequencing for the fungal isolate. Gene sequence analysis revealed that isolates A1-5, H1-1 and A6-2 were closely related to *Bacillus cereus, Streptomyces noursei* and *Rhizopus stolonifer* (accession numbers NR115714, NR115417 and AB113023, respectively) with similarity percentage of 99%, 98%, and 99%, respectively. Hence, the purified isolates were identified as *Bacillus cereus* A1-5*, Streptomyces noursei* H1-1*,* and *Rhizopus stolonifer* A6-2, respectively. Gene sequences retrieved from this study were deposited in gene bank under accession numbers MN252511, MN252512 and MN258257, respectively (Figure 1A and B, and Figure 2 A). Fortunately, this is the first study concerning with green synthesis of Ag-NPs by *Streptomyces noursei*. Although *Bacillus cereus* and *Rhizopus stolonifer* were previously used for biosynthesis of Ag-NPs, to date, there have been limited reports on the impacts of different microbial species on multifunctional biological activities of specific NPs shape.

3.2. Biosynthesis and characterization of Ag-NPs

The primary and secondary metabolites secreted by microbes are not only responsible for reducing salts (Ag$^+$) to metallic silver (Ag^0), but also act as capping and stabilizing agents (Mittal et al., 2013; Roy et al., 2019). In this study, biomass filtrate of each microbial isolates (A1-5, H1-1, and A6-2) was incubated separately with 1 mM AgNO$_3$ for 24 h in dark conditions. Color changes from colorless to yellowish-brown are the first monitor for the biosynthesis of Ag-NPs. Negative control did not exhibit any color changes. The color change could be attributed to the excitation of surface plasmon resonance (SPR). NPs formation might be related to the enzymes involved in biomass filtrates that convert nitrate

A

0.01

B

0.002
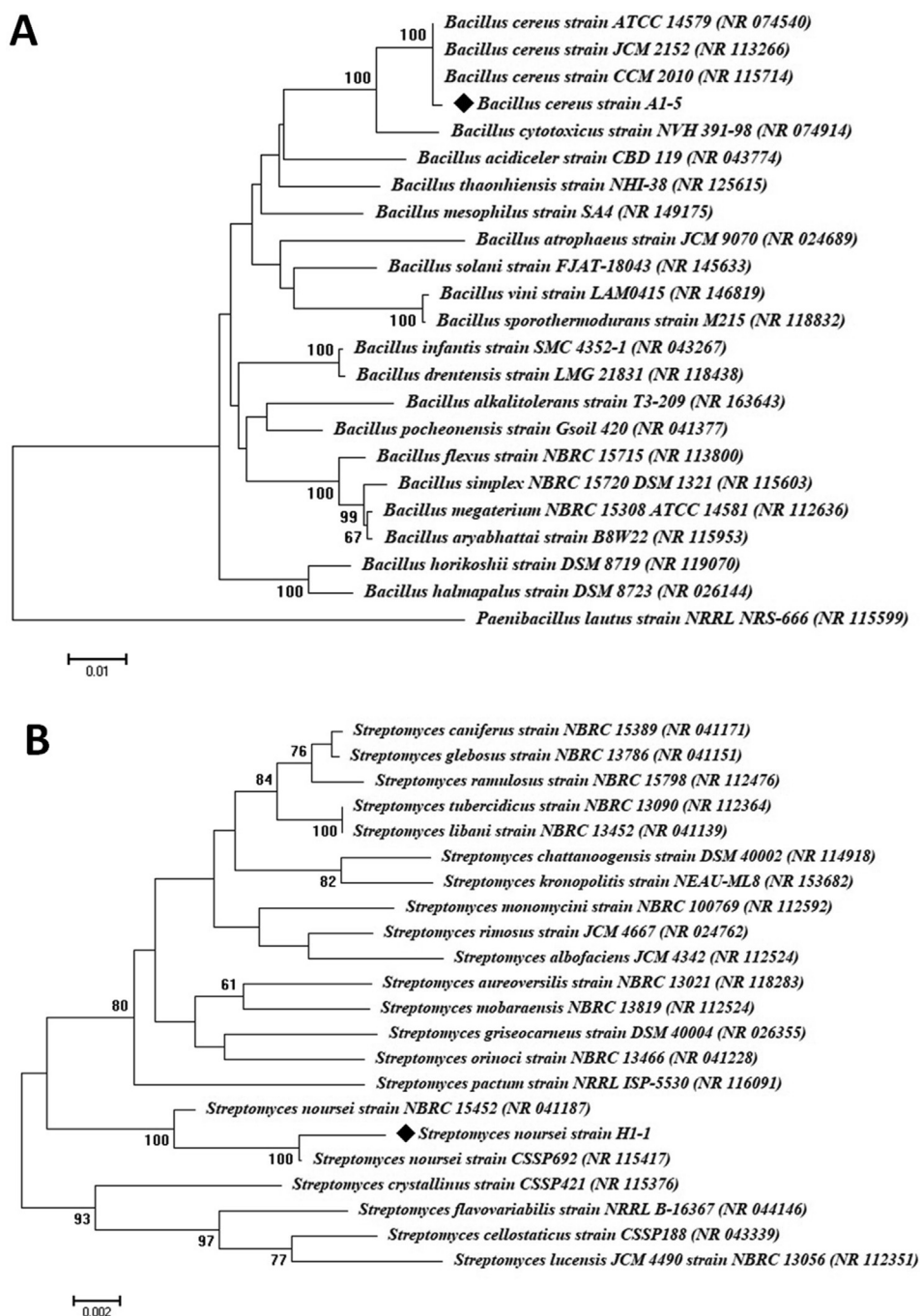
Figure 1. Phylogenetic analysis of 16S rRNA sequences of the bacterial **(A)** and actinomycete **(B)** strains with the sequences from NCBI. Symbol ◆ refers to 16S rRNA fragments retrieved from this study. The analysis was conducted with MEGA 6 using neighbor-joining method.

(NO_3^-) to nitrite (NO_2^-) and then, the electrons reduced silver ion (Ag^+) to metallic silver (Ag^0) (Khanra et al., 2015).

The Uv-*vis* spectral analysis exhibited maximum absorbance peaks at 420 nm (Figure 2 B) which may be corresponding to spherical Ag-NPs (Singh et al., 2017). In the same regard Vijaya et al. (2017) reported that, Ag-NPs synthesized by dried root suspension of *Zingiber officinale* is appeared at wavelength 425 nm as a single symmetric peak which correlated to spherical structure. The standard SPR peak of green synthesized Ag-NPs was in range 400–450 nm and any shifting in SPR peak may be attributed to biomolecules which acting as reducing and capping agent (Dong et al., 2017). Similarly, SPR peaks 400–450 nm for Ag-NPs synthesized by different microbes have been previously reported (Prakash et al., 2011; Wypij et al., 2018).

3.3. Fourier transform infra-red (FT-IR) spectroscopy

FT-IR analysis was carried out to distinguish imaginable interactions between Ag and metabolites of biomass filtrates. This may be accountable for formation, capping, stabilizing and well-dispersed Ag-NPs in colloidal solution. As indicated in Figure (3A), the FT-IR signals for the biomass filtrates (for strains A1-5, H1-1 and A6-2) showed two maximum bands at 1640 cm^{-1} and 3300 cm^{-1}. The peak at 1640 cm^{-1} (C=O, C=N, and C=C) is correspond to amide I and amide II linkages of proteins, while peak 3300 cm^{-1} is responsible for binding vibration of N–H groups (Hassan et al., 2019).

On the other hand, varied peaks were obtained for different biofabricated NPs (Figure 3A). As indicated, Ag-NPs fabricated by *Bacillus cereus* A1-5 showed two peaks at 2146 and 1392 cm^{-1} while Ag-NPs
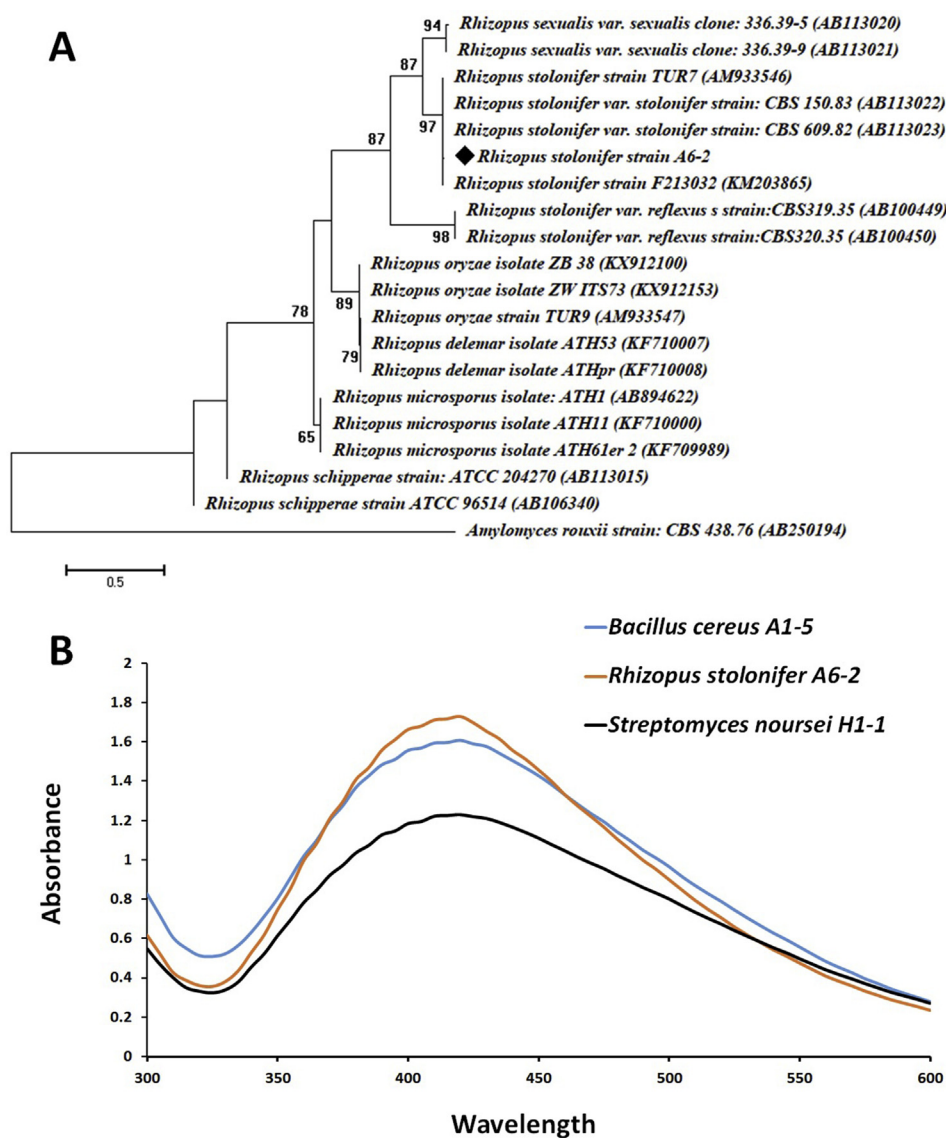
Figure 2. (A) denotes Phylogenetic analysis of ITS sequences of the fungal strain with the sequences from NCBI. Symbol ◆ refers to ITS fragments retrieved from this study. The analysis was conducted with MEGA 6 using neighbor-joining method. **(B)** denotes UV–vis spectrophotometer of Ag-NPs synthesized by *Bacillus cereus* A1-5, *Streptomyces noursei* H1-1 and *Rhizopus stolonifer* A6-2.
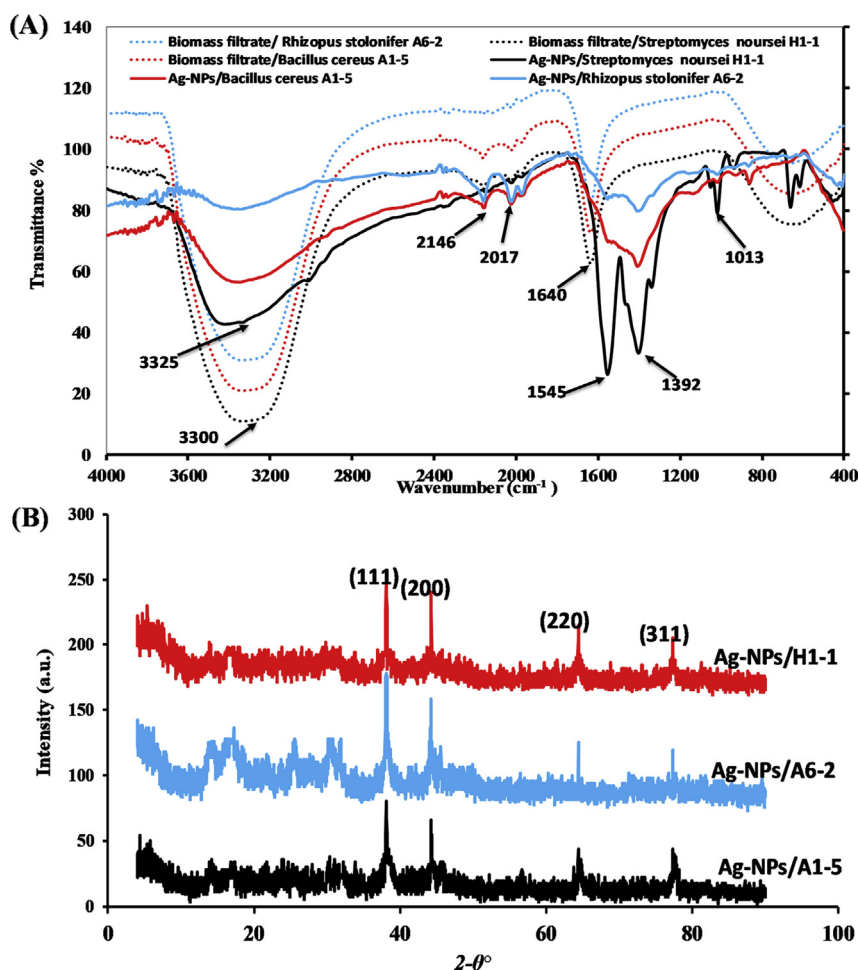
fabricated by *Streptomyces noursei* H1-1 showed four peaks at 3325, 1545, 1392, and 1013 cm^{-1} and Ag-NPs fabricated by *Rhizopus stolonifer* A6-2 showed three peaks at 2146, 1392, and 2017 cm^{-1}. The peaks at 2146 and 2017 cm^{-1} are designated to alkyne stretch (C≡C) and stretching of aldehydic amines (C–H$_2$), respectively. The band at 1545 cm^{-1} corresponds to N–H stretching of amide I band of protein. The bands observed at 1013 cm^{-1} are assigned to C–N stretching vibrations of aromatic and aliphatic amines. While common band observed at 1392 cm^{-1} is corresponding to C–H blending of aldehyde. The peak at 3325 cm^{-1} is corresponds to the O–H stretching group of alcohol or N–H stretching of secondary amine. The vibration bands of FT-IR spectra of biosynthesized Ag-NPs by different microbes and their related compound classes are shown in Table 1.

The above data indicated that reduction, stabilization, and dispersion of Ag-NPs are mainly attributed to the presence of proteins and phenols. These compounds react with Ag-NPs *via* various mechanisms including cysteine residues, amino groups or by attraction due to negative charges of carboxylic groups in exo-enzymes contained in biomass filtrate of different microorganisms (Ammar and El-Desouky, 2016; Kumar et al., 2016). Hence, it is concluded that the varied metabolites involved in

biomass filtrates of each strain (A1-5, H1-1, and A6-2) have the main role in the formation and size reduction of Ag in well-stabilized nano-form. This may also affect the functional properties and applications of the biosynthesized NPs.

3.4. X-ray diffraction patterns (XRD)

The XRD pattern of the Ag-NPs synthesized by *Bacillus cereus* A1-5, *Streptomyces noursei* H1-1, and *Rhizopus stolonifer* A6-2 was demonstrated using specific peaks located in the XRD spectra (Figure 3b). The analysis showed four diffraction peaks at $2\theta = 38.08$, 44.27, 64.41 and 77.36 that characterized the face center cubic (fcc) nano-structure of (111), (200), (220) and (311), respectively. The characterized diffraction intensity peaks are agreement with JCPDS standard No. 04–0783. Similarly, the previous studies had an indexed fcc crystallographic structure of Ag-NPS synthesized by *Bacillus spp., Streptomyces spp. and Rhizopus stolonifer* at diffraction peaks (111), (200), (220) and (300) (Fouad et al., 2017; Fouda et al., 2019a, 2019c). On the other hand, the unassigned peaks showed in XRD chart could be attributed to the crystallization of bio-organic materials that covered NPs surface (Thomas

Figure 3. (A) FT-IR spectra of biomass filtrate and Ag-NPs synthesized by *Bacillus cereus* A1-5, *Streptomyces noursei* H1-1 and *Rhizopus stolonifer* A6-2. (B) XRD pattern of Ag-NPs showed four diffraction peaks at different 2θ values.

et al., 2019). The average particle sizes of Ag-NPs reported in this study have been calculated according to Scherrer equation and were ranging between 10–55, 11–40 and 10–50 nm for those synthesized by strains *Bacillus cereus* A1-5, *Streptomyces noursei* H1-1, and *Rhizopus stolonifer* A6-2, respectively.

3.5. Transmission electron microscopy (TEM)

TEM analysis is the most effective method for detecting the morphological characters including the size and shape of synthesized Ag-NPs. TEM images of Ag-NPs synthesized by A1-5, H1-1 and A6-2 strains (Figure 4 A1, B1, and C1, respectively) showed well dispersed, spherical Ag-NPs with size ranging between 6–50nm, 6–30 and 6–40nm, respectively. The recently published studies reported the fabrication of bigger
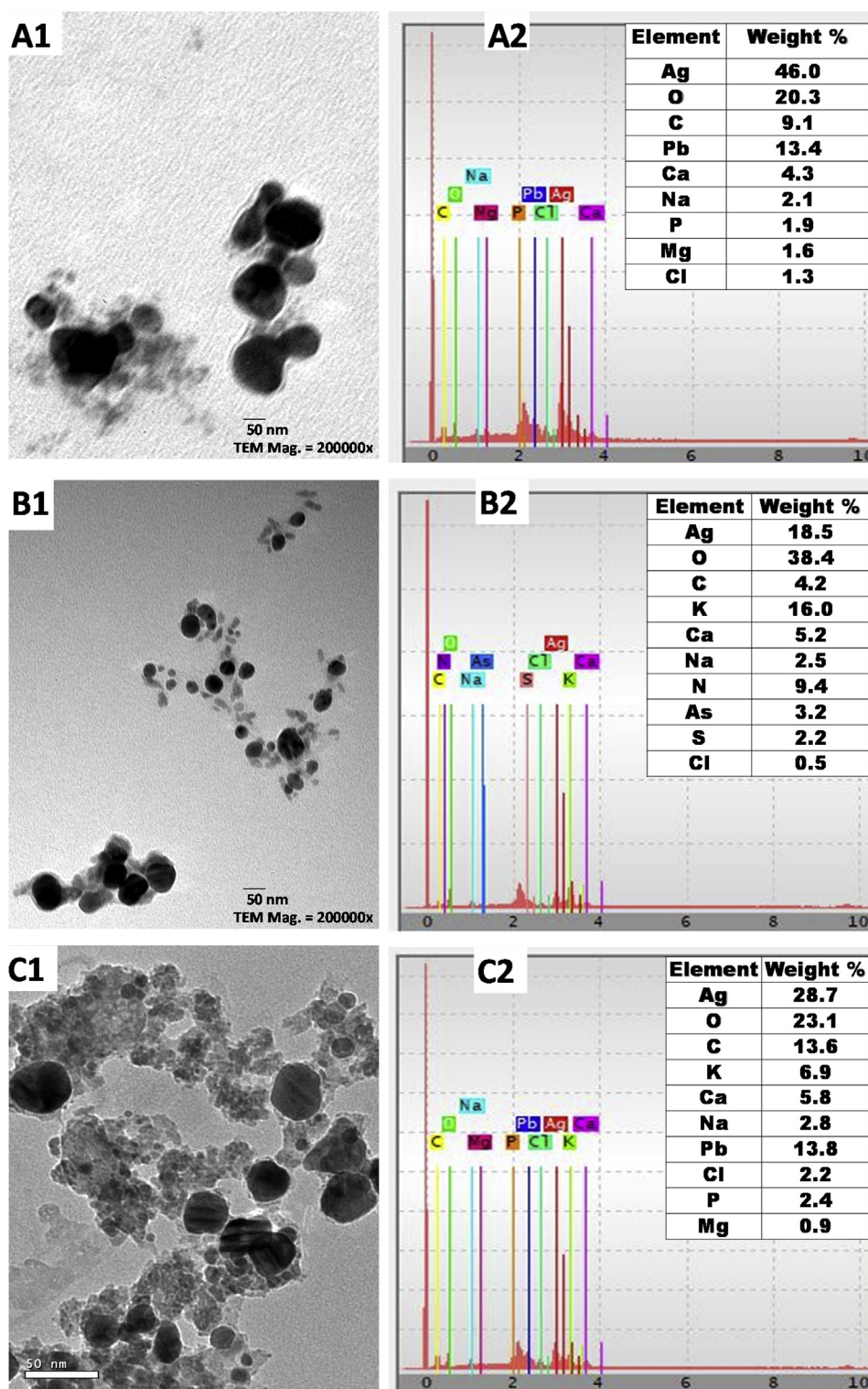
nano-silver a 63.14 nm and 88 nm for those synthesized by *Streptomyces* spp. (Fouda et al., 2019c), and *Phoma gardeniae* (Rai et al., 2014), respectively. Moreover, the activity of biosynthesized Ag-NPs was correlated with their size which enhances their biocompatibility and stability (Kim et al., 2011). These data can conclude that, the microbial species have the capacity for biosynthesis of smaller Ag-NPs as compared to the previously reported NPs.

3.6. Scanning electron microscopy (SEM-EDX)

The qualitative and quantitative elemental compositions of Ag-NPs synthesized by strains A1-5, H1-1, and A6-2 were analyzed and compared using SEM-EDX (Figure 4, A2; B2; and C2, respectively). As shown, the existence of spherical Ag-NPs with various weight percent is

Table 1. Summarize FT-IR spectral positions with their corresponding vibration modes for biomass filtrate and Ag-NPs synthesized by *Bacillus cereus* A1-5, *Streptomyces noursei* H1-1 and *Rhizopus stolonifer* A6-2.

Absorption frequency (cm^{-1})	Chemical groups	Compound class
1013	C–N stretching	Vibration of aromatic and aliphatic amines
1392	C–H bending	aldehyde
1545	N–H stretching	Vibration of amide 1 of proteins
1640	C=C stretching, C=N stretching,	Alkene, imine/oxime
2017	C–H_2 stretching	Aldehylic amine
2146	C≡C stretching	alkyne
3300	N–H stretching	Aliphatic primary amine
3325	O–H stretching, N–H stretching	Alcohol, secondary amine

Element	Weight %
Ag	46.0
O	20.3
C	9.1
Pb	13.4
Ca	4.3
Na	2.1
P	1.9
Mg	1.6
Cl	1.3

Element	Weight %
Ag	18.5
O	38.4
C	4.2
K	16.0
Ca	5.2
Na	2.5
N	9.4
As	3.2
S	2.2
Cl	0.5

Element	Weight %
Ag	28.7
O	23.1
C	13.6
K	6.9
Ca	5.8
Na	2.8
Pb	13.8
Cl	2.2
P	2.4
Mg	0.9

Figure 4. Characterization of biosynthesized Ag-NPs: (A1, B1, and C1) TEM images, (A2, B2, and C2) EDX spectra and elemental analysis for Ag-NPs biosynthesized by *Bacillus cereus* A1-5, *Streptomyces noursei* H1-1 and *Rhizopus stolonifer* A6-2, respectively.

mainly attributed due to the different reducing and stabilizing agent present in biomass filtrate of each microorganism. The elemental analysis confirmed the fabrication of Ag-NPs at the percentage of 46.0, 18.5 and 28.7% for strains A1-5, H1-1 and A6-2, respectively. EDX spectra also showed the presence of Ag-NPs peak at nearly 3 keV indicating that silver is the major element (Vijayabharathi et al., 2018). The presence of N in Ag-NPs synthesized by *Streptomyces noursei* H1-1 may be released from AgNO$_3$ (precursors). The presence of minor peaks in EDX chart such as O, C, Pb, Ca, Mg, Cl may be originated from X-ray emissions of microbial metabolites including proteins containing cysteine residues, sugars, carbohydrates, amino groups. These results are compatible with other reported microbes mediated biosynthesis of Ag-NPs (Singh et al., 2019).
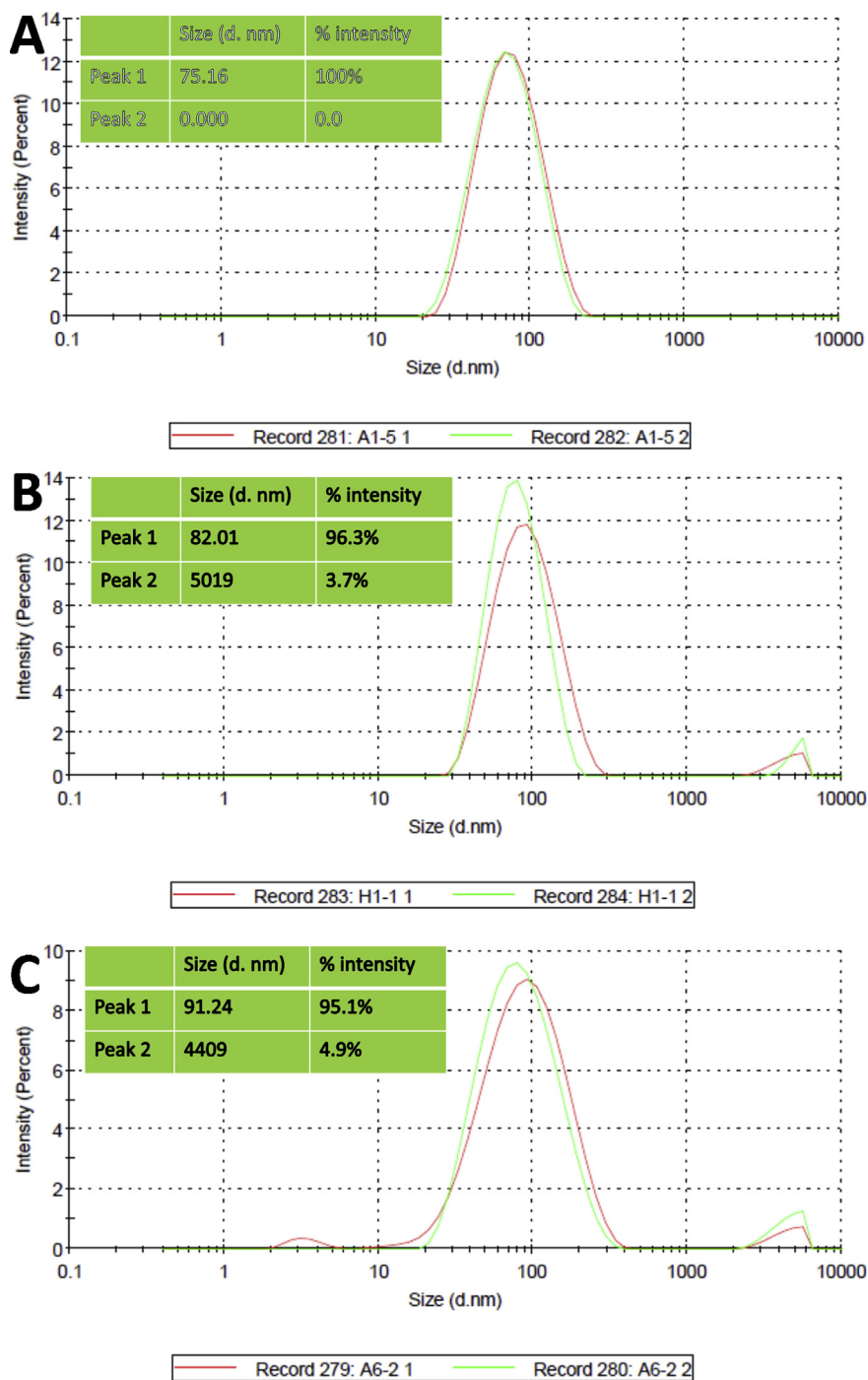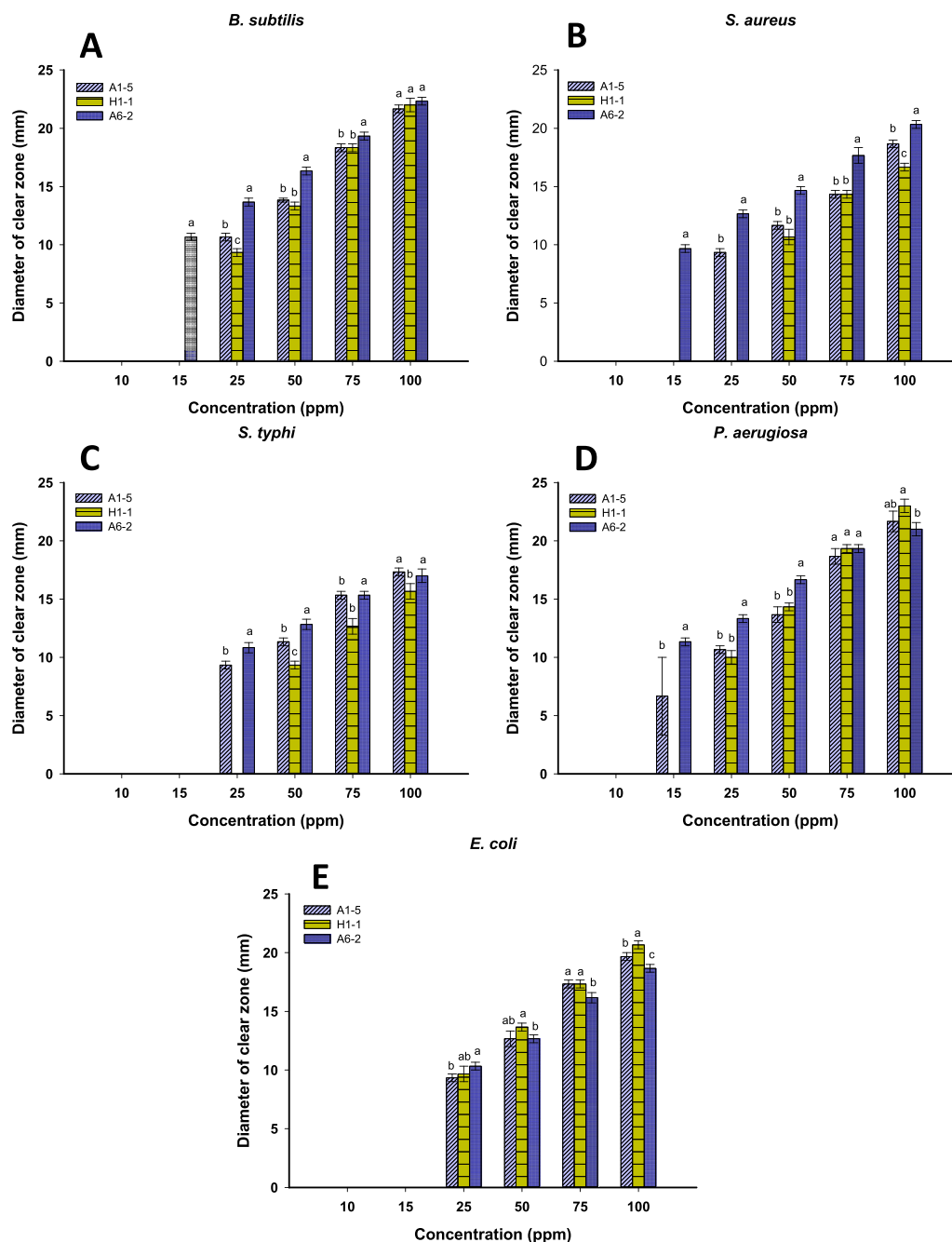
Figure 5. DLS measurement of biosynthesized Ag-NPs. A, B and C denotes Ag-NPs synthesized by *Bacillus cereus* A1-5, *Streptomyces noursei* H1-1 and *Rhizopus stolonifer* A6-2, respectively.

3.7. Dynamic light scattering (DLS) and zeta potential analysis

DLS analysis is used to measure the NPs size in colloid solutions according to the interaction between light and nanoparticles (Tomaszewska et al., 2013). Data represented in Figure 5 (A-C) showed that, the average sizes were 75.16 nm (100% intensity) for Ag-NPs synthesized by *Bacillus cereus* A1-5, while it was 82.01 nm (96.3% intensity) and 5019 nm (3.7% intensity) for NPs synthesized by *Streptomyces noursei* H1-1. On the other hand, the average particle size of Ag-NPs synthesized by *Rhizopus stolonifer* A6-2 was 91.24nm (95.1% intensity), and 4409 (4.9% intensity). According to the previous analysis of XRD, TEM, and DLS, we can conclude that, NP sizes are differed by

each analysis. Generally, NPs size obtained from DLS were bigger than those by XRD and TEM. This phenomenon can be attributed to that, DLS measurements are affected by metallic core, coating, and stabilizer substances which accumulate on NPs surface (Tomaszewska et al., 2013). On the other hand, the non-homogenous distribution of particles in the colloidal solution is due to the increased NPs size obtained by DLS analysis (Singh et al., 2017).

The stability of biosynthesized NPs was detected according to particle surface charge which measured by zeta potential analysis (Fouda et al., 2018). The high positive or negative zeta potential values (more than ± 30 mV) remain particles far from each other and hence prevent aggregations (Fouda and Shaheen, 2017; Meléndrez et al., 2010). In

Figure 6. Antibacterial activity of different concentrations (10–100 ppm) of Ag-NPs synthesized by *Bacillus cereus* A1-5*, Streptomyces noursei* H1-1 and *Rhizopus stolonifer* A6-2 against Gram-positive bacteria including: (**A**) *Bacillus subtilis* ATCC6633, (**B**) *Staphylococcus aureus* ATCC6538, and Gram-negative bacteria including: (**C**) *Salmonella typhimurium* ATCC14028, (**D**) *Pseudomonas aeruginosa* ATCC9022, and (**E**) *Escherichia coli* ATCC8739.

this study, zeta potential analysis revealed that, negative charge of Ag-NPs synthesized by *Bacillus cereus* A1-5, *Streptomyces noursei* H1-1, and *Rhizopus stolonifer* A6-2 were −17.5mV, −18.9mV and −15.6mV, respectively. The stability of Ag-NPs and the potential biomedical applications are correlated with their size and zeta potential measurements (Ge et al., 2014).

3.8. Properties of biosynthesized Ag-NPs

3.8.1. Antibacterial activity

The antibacterial activities of silver-based NPs synthesized by strains A1-5, H1-1 and A6-2 were evaluated and compared. Biomass filtrate of different microbial strains (as control) did not exhibit any antibacterial

activities indicating the absence of any active antimicrobial metabolites. On the other hand, Ag-NPs have demonstrated a potent antibacterial effect against representative Gram-negative and Gram-positive bacterial human pathogens. The bactericidal effect was increased by increasing NPs concentration (Figure 6). These results proved the potential use of Ag-NPs as antibacterial agents with broad-spectrum activity. Our results are consistent with that obtained by Fouda et al. (2017).

Among the examined bacteria, *P. aeruginosa* was the most sensitive strain for Ag-NPs. This stronger activity of NPs on Gram-negative bacteria is mainly attributed to the thicker peptidoglycan cell wall (30 nm) of Gram-positive bacteria than Gram-negative cell wall (3–4 nm) (Chatterjee et al., 2015). Ag-NPs are possibly adhering to bacterial cell walls and infiltrate into it causing physical damage, and

consequently leakage of cellular constituents and bacterial death (Khalandi et al., 2017). Besides, enhanced adhesion of NPs to cell walls may have attributed to its positive surface charge, which is electrostatically attracted to the negatively charged microbial cell membrane. This would lead to some morphological changes characterized by cytoplasmic shrinkage, membrane detachment and ultimately cell wall rupture (Nalwade and Jadhav, 2013). Moreover, the Ag^+ ions released from Ag-NPs might permeate into the bacterial cell, prohibiting additional replication or formation of cellular components such as protein, DNA and peptidoglycan (Chaloupka et al., 2010; Morones et al., 2005).

At the lowest concentration (10 ppm), there was no activity of Ag-NPs against any bacterial strains. Ag-NPs synthesized by *R. stolonifer* A6-2 is more effective against Gram-positive bacteria than those synthesized by A1-5 and H1-1. Meanwhile, *B. subtilis* was the most sensitive Gram-positive bacteria for the three biogenic Ag-NPs. At 75 ppm, NPs synthesized by strains A6-2 and H1-1 showed equal activities against *P. aeruginosa* with clear zones of 19.3 mm. As well, NPs produced by strains A6-2 and A1-5 have exhibited equal effectiveness against *S. typhimurium* with clear zones of 15.3 mm. At 100 ppm, the Ag-NPs fabricated by H1-1 has exhibited the maximum antibacterial activity against *P. aeruginosa* with a clear zone of 23 ± 1.0 mm. At concentrations greater than 25 ppm, Ag-NPs synthesized by H1-1 was the most active against *E. coli*.

The strong activities of H1-1 nano-molecules against some tested pathogenic bacteria may be due to its size which being smaller than those produced by A6-2 and A1-5 (6–30, 6–40 and 6–50 nm, respectively). Smaller sized nanoparticles have a larger surface area and their agglomeration around the microbial cell wall lead to prevent their division (Siddiqi et al., 2018). In line with our results Das et al. (2011) reported the premium inhibitory effect of the small size Ag-NPs against certain bacteria.

The MIC values (Figure 6) of biogenic Ag-NPs against prokaryotic pathogens was low in the range of 15 and 25 ppm. While it increased to 50 ppm for NPs synthesized by strain H1-1 against the Gram-negative *S. aureus* and *S. typhimurium*. The MIC for Ag-NPs/A6-2 against Gram-positive and *P. aeruginosa* was 15ppm with inhibition zones ranging from 9.5–11.5 mm. However, the MIC for Ag-NPs/A6-2 against *E. coli* and *S. typhimurium* was 25 ppm and recorded inhibition zones of 10.33 mm and 10.38 mm, respectively. Although the MIC for Ag-NPs/A1-5 against all pathogenic tested microbes was 25 ppm, it achieved inhibition zones ranged from 9.3–10.6 mm. This value was reduced to 15 ppm against *P. aeruginosa* with a 7.5 mm inhibition zone. The concentration of 25 ppm was considered as the MIC for Ag-NPs/H1-1 against *B. subtilis*, *E. coli* and *P. aeruginosa* with corresponding inhibition zones at 9.3, 9.6 and 10.0mm, respectively. However, the MIC for Ag-NPs/H1-1 against *S. aureus* and *S. typhimurium* was 50 ppm with the inhibition zones of 10.6 and 9.3mm, respectively.

3.8.2. Cell viability and cytotoxicity effect

Application of chemical compounds as insecticides or drugs have exhibited various cytotoxic mechanisms such as irreversible binding to certain receptors, disrupting cell membranes and preventing protein synthesis, etc. On the other hand, besides the premium antimicrobial characteristics of Ag-NPs, they have vastly reached our daily lives for producing antitumor drugs carriers, wound plasters, antimicrobial fabrics, health care, and cosmetic products. Recently, the inescapable human exposure to these nanomaterials has appointed advanced concerns about their possible risks to health, safety and eco-friendly (Liao et al., 2019) especially that Ag-NPs could be assimilated by cells either through phagocytosis, endocytosis or diffusion (Zhang et al., 2015). Therefore, the cytotoxicity test is one of the most remarkable indicators of biological assessment for safe application of biosynthesized NPs (Aslantürk, 2018).

In the current study, normal Vero cells and cancer cells (Caco-2) were incubated with different concentrations of the biogenic silver-based nanoparticles and the biogenic $AgNO_3$ for 48 h. The cytotoxic effects

were evaluated and compared using MTT assay as shown in Figure (7). As indicated, a dose-dependent (0.49–1000 μg/ml) cytotoxic effect was observed on both cancer and normal cells. Interestingly, a significant difference in the cytotoxicity was achieved between Ag-NPs and $AgNO_3$ for all concentrations. $AgNO_3$ and Ag-NPs synthesized by A1-5, H1-1 and A6-2 exhibited IC50 at 304.8 ± 21.3, 290.2 ± 14.7, 511.7 ± 68.5 and 259.0 ± 6.4 μg/ml, respectively for normal cell line (Vero cell, Figure 7A). Interestingly, they exhibited IC50 of 131.4 ± 8.5, 8.9 ± 0.5, 5.6 ± 3.0, 11.2 ± 0.5 μg/ml, respectively against Caco-2 cancer cells (Figure 7B). Accordingly, the normal Vero cells are less susceptible to nanoparticle treatments compared to the chemical silver nitrate. On the other hand, Ag-NPs at low concentrations (5.6–11.2 μg/ml) have reduced the mitochondrial function of cancer cells by 50 %. The viability of Caco-2 cells was reduced when exposed to higher $AgNO_3$ concentrations.

Previously, Paknejadi et al. (2018) assessed the efficacy of Ag-NPs on normal human skin fibroblast cell lines and reported a significant time and concentration-dependent mode in the reduction of cell viability. Also, Ag-NPs proved cytotoxic effect against the cancer cell line (MCF-7) while it was non-toxic towards the normal cell line (L-929 fibroblast cells) (Khorrami et al., 2018). On the other hand Dziedzic et al. (2016), reported the potency of Ag-NPs at 5.19 μg/ml to inhibit 50% of oral squamous cancer cell line (SCC-25) growth, after two-day incubation. Based on the results of the present study, silver nanoparticles have selective toxicity against cancer cells. This feature can be used as an effective cancer control strategy.

In the current study, TEM analysis proved the small size of the three types of biogenic Ag-NPs, which may be one of the reasons for the increased cytotoxicity of these molecules. Albers et al. (2013) and co-authors examined the toxicity of three different sized Ag-NPs on various cell lines and reported stronger cytotoxicity of the smaller particles on osteoblast. This might be due to the inverse relationship between the size and surface area of silver ions released from Ag-NPs (Albers et al., 2013). After entering the cytoplasm, silver nanoparticles themselves or silver ions can generate ROS, causing protein denaturation, DNA damage and apoptosis (Akter et al., 2018; Chernousova and Epple, 2013). Other studies reported that the entry of Ag-NPs causes disturbance of cytoplasmic membrane and leads to a generation of ROS and increased leakage of lactate dehydrogenase boosting cytotoxicity of various human cancerous cells (Park et al., 2017).

3.8.3. Insecticidal bioassay

Control of mosquitos have been established by various compounds including essential oil (Amer and Mehlhorn, 2006), plant extract (Maheswaran et al., 2008), pure plant-based compounds (Khanna et al., 2011). Recently, biosynthesized Ag-NPs have attracted great interest as a control agent. The larvicidal activities of Ag-NPs synthesized by strains A1-5, H1-1, and A6-2 were investigated on the 3rd larval instar of *Aedes aegypti* (Table 2).

Data analysis revealed that there is no significant difference in activity between high NPs concentrations (75 and 100ppm) causing 100% larval mortality (Table 2). At 50ppm, spherical Ag-NPs synthesized by strains A1-5, H1-1 and A6-2 showed larval mortality percentages at 94.7 ± 0.58, 92.7 ± 1.52 and 91.0 ± 2.0 %, respectively. At low NPs concentration (5ppm), the highest larval mortality was achieved by Ag-NPs synthesized by *Bacillus cereus A1-5* (40.0 ± 1.0 %) followed by those synthesized by *Rhizopus stolonifer* A6-2 (38.7 ± 2.89 %) and *Streptomyces noursei* H1-1 (31.7 ± 1.16 %).

On the other hand, the highest pupal mortality was achieved using 20 ppm Ag-NPs synthesized by *Streptomyces noursei* H1-1. Generally, the activities of spherical NPs synthesized by strain H1-1 on pupa at a moderate concentration (20, 25 and 50ppm) were better than those synthesized by other microbial strains. This phenomenon may be attributed to the size of NPs synthesized by actinobacteria (Fouda et al., 2019c).

To the best of our knowledge, there are a few articles follow the effect of Ag-NPs on the adult mosquito. In this context, we can conclude that

A

B
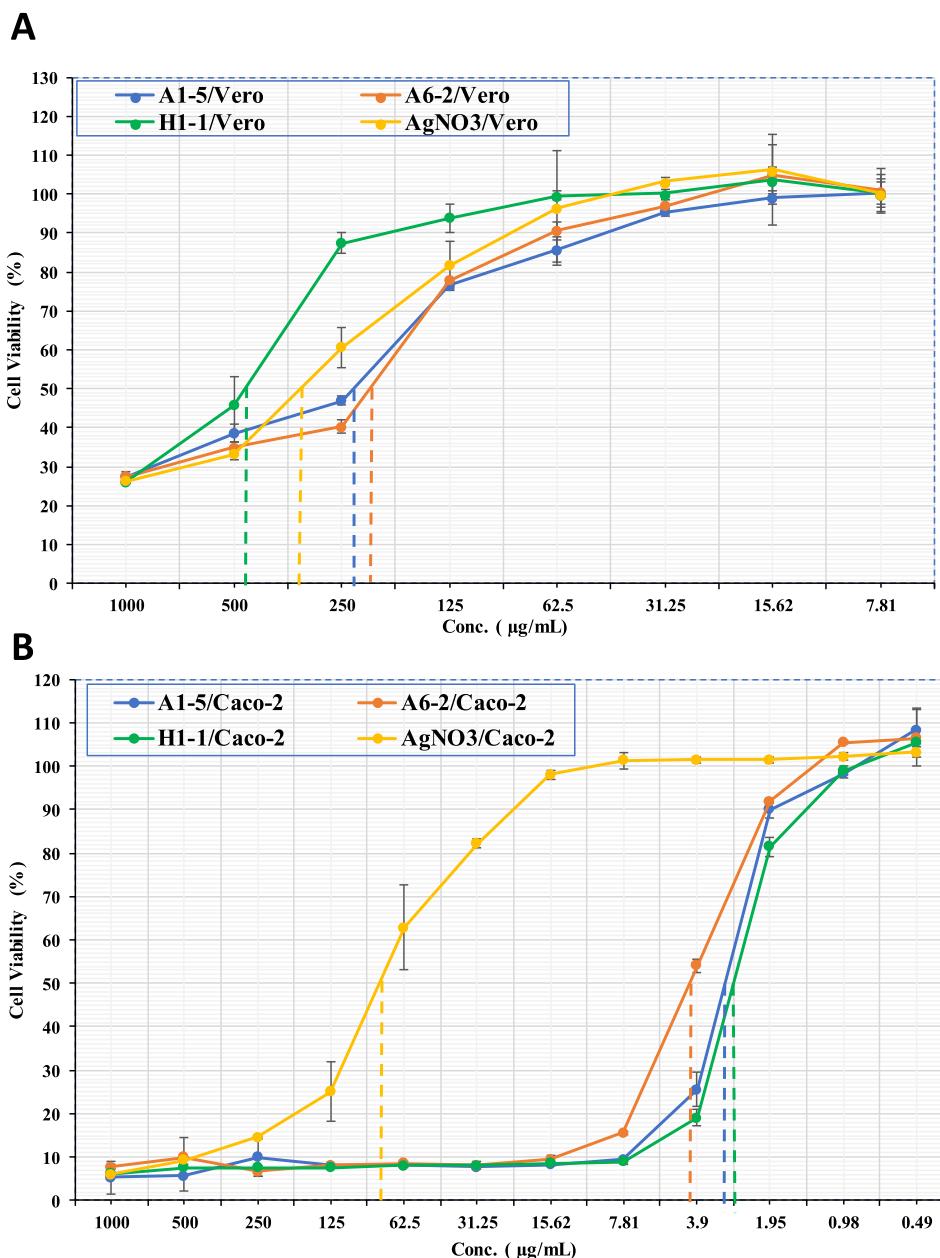
Figure 7. MTT assay of AgNO$_3$ and Ag-NPs synthesized by *Bacillus cereus A1-5, Streptomyces noursei* H1-1 and *Rhizopus stolonifer* A6-2. Against (A), normal Vero cell; (B), cancer Caco-2 cell.

Table 2. Insecticidal efficacy for Ag-NPs synthesized using *Bacillus cereus* A1-5, *Streptomyces noursei* H1-1 and *Rhizopus stolonifer* AA6-2.

Ag-NPs conc. (ppm)	Larval mortality (%)			Pupal mortality (%)			Adult emergency (%)		
	Bacillus cereus A1-5	*Streptomyces noursei* H1-1	*Rhizopus stolonifer* A6-2	*Bacillus cereus* A1-5	*Streptomyces noursei* H1-1	*Rhizopus stolonifer* A6-2	*Bacillus cereus* A1-5	*Streptomyces noursei* H1-1	*Rhizopus stolonifer* A6-2
100	100 ± 0.0[a]	100 ± 0.0[a]	100 ± 0.0[a]	0.0 ± 0.0[a]	0.0 ± 0.0[a]	0.0 ± 0.0[a]	0.0 ± 0.0[a]	0.0 ± 0.0[a]	0.0 ± 0.0[a]
75	100 ± 0.0[a]	99.7 ± 0.57[a]	99.0 ± 1.0[a]	0.0 ± 0.0[a]	0.3 ± 0.57[a]	0.67 ± 0.58[a]	0.0 ± 0.0[a]	0.0 ± 0.0[a]	0.3 ± 0.58[a]
50	94.7 ± 0.58[a]	92.7 ± 1.52[a]	91.0 ± 2.0[a]	1.7 ± 0.56[c]	4.0 ± 1.0[a]	2.3 ± 0.58[b]	3.7 ± 1.12[b]	3.3 ± 1.53[b]	6.7 ± 2.52[a]
25	90.7 ± 1.16[a]	86.0 ± 1.0[b]	86.7 ± 1.53[b]	2.3 ± 0.58[b]	4.0 ± 0.0[a]	3.7 ± 0.58[a]	7.0 ± 1.0[b]	10.0 ± 1.0[a]	9.7 ± 2.08[a]
20	78.7 ± 1.52[a]	74.7 ± 1.53[b]	71.0 ± 2.65[c]	4.0 ± 1.0[c]	7.3 ± 0.58[a]	5.7 ± 0.58[b]	17.3 ± 2.31[b]	18.0 ± 1.73[b]	23.3 ± 3.05[a]
15	60.0 ± 1.0[a]	58.7 ± 1.53[a]	59.0 ± 2.64[a]	3.0 ± 0.0[c]	4.0 ± 1.0[b]	5.7 ± 0.58[a]	37.0 ± 1.0[a]	37.3 ± 2.31[a]	36.7 ± 0.58[a]
10	49.0 ± 2.64[a]	45.3 ± 1.53[b]	46.3 ± 3.22[ab]	4.0 ± 1.0[a]	4.3 ± 0.58[a]	4.0 ± 1.0[a]	47.0 ± 3.46[a]	50.3 ± 1.16[a]	49.7 ± 3.22[a]
5	40.0 ± 1.0[a]	31.7 ± 1.16[b]	38.7 ± 2.89[a]	5.3 ± 1.5[a]	2.3 ± 0.58[b]	2.7 ± 0.58[b]	54.7 ± 2.08[c]	66.0 ± 1.0[a]	58.7 ± 2.31[b]

For each experiment, values within each three column with different letters are significantly different ($P \le 0.05$) by Tukey's test, values are mean ± SD ($n = 3$).

larvae and pupa of *Aedes aegypti* are more sensitive for high NPs concentration and this sensitivity is reduced at low concentration, hence adult mosquito is released. Data analysis showed that LC50 for Ag-NPs synthesized by strains A1-5, H1-1 and A6-2 on 3rd larval instar were 12.5, 12.8 and 12.7 ppm, respectively.

Unfortunately, the larvicidal mechanisms of Ag-NPs are still unknown, therefore, furture investigation are required to clarify the exact mechanism. One explanation suggests that, the interaction of Ag-NPs with cell molecules after penetrating through the larval membrane is causing larvae death (Elfeky et al., 2020; Sundaravadivelan and Nalini, 2012). Moreover, penetration of Ag-NPs to epithelial midgut membranes causing enzymes inactivation and hence peroxidase is released leading to cell death (Raffi et al., 2008).

4. Conclusion

In this study, three different microbial strains (*Bacillus cereus, Streptomyces noursei*, and *Rhizopus stolonifer*) were isolated from soil samples and used separately for extracellular synthesis of Ag-NPs. Color changes from colorless to yellowish-brown besides UV-*Vis* spectroscopy, FT-IR, XRD, SEM-EDX, TEM, DLS and zeta potential analysis were used for physicochemical characterization. These microbes have mediated the biosynthesize of spherical Ag-NPs with varied sizes ranging from 6–50 nm exhibiting maximum absorbance peaks at 420 nm, crystal-metallic in nature, well dispersed and more stable with highly negative zeta potential values. Nano-silver exhibits varied antibacterial activity against pathogenic Gram-negative and Gram-positive bacteria. Besides this, the biosynthesized Ag-NPs showed varied concentration dependent biological activities including *in-vitro* cytotoxicity against Caco-2 cancer cell line and larvicidal activity against dengue vector *Aedes aegypti*. This study illustrated the importance and effect of metabolites secreted by specific microbial strain on the fabrication and specific functional biological properties of the biosynthesized NPs materials.

Declarations

Author contribution statement

Sultan M. Alsharif: Analyzed and interpreted the data; Performed the experiments; Contributed reagents, materials, analysis tools or data.

Salem S. Salem: Conceived and designed the experiments; Performed the experiments; Analyzed and interpreted the data; Contributed reagent, material, analysis tools or data; Wrote the paper.

Mohamed A. Abdel-Rahman, Saad E. Hassan: Conceived and designed the experiments; Analyzed and interpreted the data; Wrote the paper.

Amr Fouda: Conceived and designed the experiments; Performed the experiments; Analyzed and interpreted the data; Contributed reagents, materials, analysis tools or data; Wrote the paper.

Ahmed M. Eid: Conceived and designed the experiment; Analyzed and interpreted the data; Wrote the paper.

Mohamed A. Awad: Conceived and designed the experiments; Performed the experiments; Analyzed and interpreted the data.

Asem A. Mohamed: Conceived and designed the experiments; Analyzed and interpreted the data; Performed the experiments; Contributed reagents, materials, analysis tools or data.

Competing interest statement

The authors declare no conflict of interest.

References

Ammar, H., El-Desouky, T., 2016. Green synthesis of nanosilver particles by *Aspergillus terreus* HA 1N and *Penicillium expansum* HA 2N and its antifungal activity against mycotoxigenic fungi. J. Appl. Microbiol. 121, 89–100.

Abbott, W.S., 1925. A method of computing the effectiveness of an insecticide. J. Econ. Entomol. 18, 265–267.

Akter, M., Sikder, M.T., Rahman, M.M., Ullah, A.A., Hossain, K.F.B., Banik, S., et al., 2018. A systematic review on silver nanoparticles-induced cytotoxicity: physicochemical properties and perspectives. J. Adv. Res. 9, 1–16.

Al-Shmgani, H.S., Mohammed, W.H., Sulaiman, G.M., Saadoon, A.H., 2017. Biosynthesis of silver nanoparticles from *Catharanthus roseus* leaf extract and assessing their antioxidant, antimicrobial, and wound-healing activities. Artif. Cells Nanomed. Biotechnol. 45, 1234–1240.

Albers, C.E., Hofstetter, W., Siebenrock, K.A., Landmann, R., Klenke, F.M., 2013. *In vitro* cytotoxicity of silver nanoparticles on osteoblasts and osteoclasts at antibacterial concentrations. Nanotoxicology 7, 30–36.

Amer, A., Mehlhorn, H., 2006. Larvicidal effects of various essential oils against Aedes, Anopheles, and Culex larvae (Diptera, Culicidae). Parasitol. Res. 99, 466–472.

Aslantürk, Ö.S., 2018. In Vitro Cytotoxicity and Cell Viability Assays: Principles, Advantages, and Disadvantages, 2. InTech.

Chaloupka, K., Malam, Y., Seifalian, A.M., 2010. Nanosilver as a new generation of nanoproduct in biomedical applications. Trends Biotechnol. 28, 580–588.

Chatterjee, T., Chatterjee, B.K., Majumdar, D., Chakrabarti, P., 2015. Antibacterial effect of silver nanoparticles and the modeling of bacterial growth kinetics using a modified Gompertz model. Biochim. Biophys. Acta Gen. Subj. 1850, 299–306.

Chernousova, S., Epple, M., 2013. Silver as antibacterial agent: ion, nanoparticle, and metal. Angew. Chem. Int. Ed. 52, 1636–1653.

Das, R., Gang, S., Nath, S.S., 2011. Preparation and antibacterial activity of silver nanoparticles. J. Biomaterials Nanobiotechnol. 2, 472.

Devi, J., Bhimba, B., 2012. Anticancer activity of silver nanoparticles synthesized by the seaweed *ulva lactuca in vitro*. Open Access Sci. Rep. 1 (4), 242.

Dong, Z.-Y., Rao, N., Prabhu, M., Xiao, M., Wang, H.-F., Hozzein, W.N., et al., 2017. Antibacterial activity of silver nanoparticles against *Staphylococcus warneri* synthesized using endophytic bacteria by photo-irradiation. Front. Microbiol. 8, 1090.

Dziedzic, A., Kubina, R., Bułdak, R., Skonieczna, M., Cholewa, K., 2016. Silver nanoparticles exhibit the dose-dependent anti-proliferative effect against human squamous carcinoma cells attenuated in the presence of berberine. Molecules 21, 365.

Elfeky, A.S., Salem, S.S., Elzaref, A.S., Owda, M.E., Eladawy, H.A., Saeed, A.M., et al., 2020. Multifunctional cellulose nanocrystal/metal oxide hybrid, photo-degradation, antibacterial and larvicidal activities. Carbohydr. Polym. 230, 115711.

Fouad, H., Hongjie, L., Yanmei, D., Baoting, Y., El-Shakh, A., Abbas, G., et al., 2017. Synthesis and characterization of silver nanoparticles using *Bacillus amyloliquefaciens* and *Bacillus subtilis* to control filarial vector *Culex pipiens* pallens and its antimicrobial activity. Artif. Cells Nanomed. Biotechnol. 45, 1369–1378.

Fouda, A., Shaheen, TI, 2017. Silver Nanoparticles: biosynthesis, characterization and application on cotton fabrics. Microbiol. Res. J. Int. 1–14.

Fouda, A.H., Hassan, S.E.-D., Eid, A.M., Ewais, E.E.-D., 2015. Biotechnological applications of fungal endophytes associated with medicinal plant *Asclepias sinaica* (Bioss.). Ann. Agric. Sci. 60, 95–104.

Fouda, A., El-Din Hassan, S., Salem, S.S., Shaheen, T.I., 2018. *In-Vitro* cytotoxicity, antibacterial, and UV protection properties of the biosynthesized Zinc oxide nanoparticles for medical textile applications. Microb. Pathog. 125, 252–261.

Fouda, A., Abdel-Maksoud, G., Abdel-Rahman, M.A., Eid, A.M., Barghoth, M.G., El-Sadany, M.A.-H., 2019a. Monitoring the effect of biosynthesized nanoparticles against biodeterioration of cellulose-based materials by *Aspergillus niger*. Cellulose 26, 6583–6597.

Fouda, A., Abdel-Maksoud, G., Abdel-Rahman, M.A., Salem, S.S., Hassan, S.E.-D., El-Sadany, M.A.-H., 2019b. Eco-friendly approach utilizing green synthesized nanoparticles for paper conservation against microbes involved in biodeterioration of archaeological manuscript. Int. Biodeterior. Biodegrad. 142, 160–169.

Fouda, A., Hassan, S.E.-D., Abdo, A.M., El-Gamal, M.S., 2019c. Antimicrobial, Antioxidant and Larvicidal activities of spherical silver nanoparticles synthesized by endophytic *Streptomyces* Spp. Biological Trace Element Research. 195(2), pp. 707–724.

Fouda, A., Saad, E., Elgamal, M.S., Mohmed, A.A., Salem, S.S., 2017. Optimal factors for biosynthesis of silver nanoparticles by *Aspergillus* sp. Azhar Bull. Sci. 9, 161–172.

Ge, L., Li, Q., Wang, M., Ouyang, J., Li, X., Xing, M.M., 2014. Nanosilver particles in medical applications: synthesis, performance, and toxicity. Int. J. Nanomed. 9, 2399.

Gupta, R.K., Kumar, V., Gundampati, R.K., Malviya, M., Hasan, S.H., Jagannadham, M.V., 2017. Biosynthesis of silver nanoparticles from the novel strain of *Streptomyces* sp. BHUMBU-80 with highly efficient electroanalytical detection of hydrogen peroxide and antibacterial activity. J. Environ. Chem. Eng. 5, 5624–5635.

Hassan, S.E.-D., Salem, S.S., Fouda, A., Awad, M.A., El-Gamal, M.S., Abdo, A.M., 2018. New approach for antimicrobial activity and bio-control of various pathogens by biosynthesized copper nanoparticles using endophytic actinomycetes. J. Radiat. Res. Appl. Sci. 11, 262–270.

Hassan, S.E.-D., Fouda, A., Radwan, A.A., Salem, S.S., Barghoth, M.G., Awad, M.A., et al., 2019. Endophytic actinomycetes *Streptomyces* spp. mediated biosynthesis of copper oxide nanoparticles as a promising tool for biotechnological applications. JBIC J. Biol. Inorg. Chem. 24, 377–393.

Khalandi, B., Asadi, N., Milani, M., Davaran, S., Abadi, A.J.N., Abasi, E., et al., 2017. A review on potential role of silver nanoparticles and possible mechanisms of their actions on bacteria. Drug Res. 11, 70–76.

Khanna, V.G., Kannabiran, K., Rajakumar, G., Rahuman, A.A., Santhoshkumar, T., 2011. Biolarvicidal compound gymnemagenol isolated from leaf extract of miracle fruit plant, Gymnema sylvestre (Retz) Schult against malaria and filariasis vectors. Parasitol. Res. 109, 1373.

Khanra, K., Panja, S., Choudhuri, I., Chakraborty, A., Bhattacharyya, N., 2015. Evaluation of antibacterial activity and cytotoxicity of green synthesized silver nanoparticles using *Scoparia dulcis*. Nano Biomed. Eng. 7, 128–133.

Khorrami, S., Zarrabi, A., Khaleghi, M., Danaei, M., Mozafari, M., 2018. Selective cytotoxicity of green synthesized silver nanoparticles against the MCF-7 tumor cell line and their enhanced antioxidant and antimicrobial properties. Int. J. Nanomed. 13, 8013.

Kim, S.-H., Lee, H.-S., Ryu, D.-S., Choi, S.-J., Lee, D.-S., 2011. Antibacterial activity of silver-nanoparticles against *Staphylococcus aureus* and *Escherichia coli*. Kor. J. Microbiol. Biotechnol. 39, 77–85.

Kumar, B., Smita, K., Seqqat, R., Benalcazar, K., Grijalva, M., Cumbal, L., 2016. *In vitro* evaluation of silver nanoparticles cytotoxicity on Hepatic cancer (Hep-G2) cell line and their antioxidant activity: green approach for fabrication and application. J. Photochem. Photobiol. B Biol. 159, 8–13.

Lane, D., 1991. 16S/23S rRNA sequencing. Nucleic acid techniques in bacterial systematics, pp. 115–175.

Liao, C., Li, Y., Tjong, S.C., 2019. Bactericidal and cytotoxic properties of silver nanoparticles. Int. J. Mol. Sci. 20, 449.

Luo, K., Jung, S., Park, K.-H., Kim, Y.-R., 2018. Microbial biosynthesis of silver nanoparticles in different culture media. J. Agric. Food Chem. 66, 957–962.

Maheswaran, R., Sathish, S., Ignacimuthu, S., 2008. Larvicidal Activity of *Leucas aspera* (Willd.) against the Larvae of *Culex quinquefasciatus* Say. And *Aedes aegypti* L. International Journal of Integrative Biology.

Malik, M.A., O'Brien, P., Revaprasadu, N., 2002. A simple route to the synthesis of core/shell nanoparticles of chalcogenides. Chem. Mater. 14, 2004–2010.

Meléndrez, M., Cárdenas, G., Arbiol, J., 2010. Synthesis and characterization of gallium colloidal nanoparticles. J. Colloid Interface Sci. 346, 279–287.

Miller, D., Bryant, J., Madsen, E., Ghiorse, W., 1999. Evaluation and optimization of DNA extraction and purification procedures for soil and sediment samples. Appl. Environ. Microbiol. 65, 4715–4724.

Mittal, A.K., Chisti, Y., Banerjee, U.C., 2013. Synthesis of metallic nanoparticles using plant extracts. Biotechnol. Adv. 31, 346–356.

Mohamed, A.A., Fouda, A., Elgamal, M.S., EL-Din Hassan, S., Shaheen, T.I., Salem, S.S., 2017. Enhancing of cotton fabric antibacterial properties by silver nanoparticles synthesized by new Egyptian strain *Fusarium keratoplasticum* A1-3. Egypt. J. Chem. 60, 63–71.

Mohamed, A.A., Fouda, A., Abdel-Rahman, M.A., Hassan, S.E.-D., El-Gamal, M.S., Salem, S.S., et al., 2019. Fungal strain impacts the shape, bioactivity and multifunctional properties of green synthesized zinc oxide nanoparticles. Biocataly. Agric. Biotechnol. 19, 101103.

Mohmed, A.A., Saad, E., Fouda, A., Elgamal, M.S., Salem, S.S., 2017. Extracellular biosynthesis of silver nanoparticles using *Aspergillus* sp. and evaluation of their antibacterial and cytotoxicity. J. Appl. Life Sci. Int. 11, 1–12.

Morejón, B., Pilaquinga, F., Domenech, F., Ganchala, D., Debut, A., Neira, M., 2018. Larvicidal activity of silver nanoparticles synthesized using extracts of *ambrosia arborescens* (asteraceae) to control *Aedes aegypti* L.(Diptera: Culicidae). J. Nanotechnol. 2018.

Morones, J.R., Elechiguerra, J.L., Camacho, A., Holt, K., Kouri, J.B., Ramírez, J.T., et al., 2005. The bactericidal effect of silver nanoparticles. Nanotechnology 16, 2346.

Mukherjee, S., Chowdhury, D., Kotcherlakota, R., Patra, S., 2014. Potential theranostics application of bio-synthesized silver nanoparticles (4-in-1 system). Theranostics 4, 316.

Nalwade, A.R., Jadhav, A., 2013. Biosynthesis of silver nanoparticles using leaf extract of *Datura alba Nees*. and evaluation of their antibacterial activity. Arch. Appl. Sci. Res. 5, 45–49.

Organization, W.H., 1996. Report of a WHO Consultation on Public Health Issues Related to Human and Animal Transmissible Spongiform Encephalopathies, Geneva, Swtizerland, 2-3 April 1996. World Health Organization, Geneva.

Organization, W.H., 2016. Dengue Y Dengue Grave.

Paknejadi, M., Bayat, M., Salimi, M., Razavi, V., 2018. Concentration-and time-dependent cytotoxicity of silver nanoparticles on normal human Skin fibroblast cell line. Iran. Red Crescent Med. J. 20.

Park, J.H., Gurunathan, S., Choi, Y.-J., Han, J.W., Song, H., Kim, J.-H., 2017. Silver nanoparticles suppresses brain-derived neurotrophic factor-induced cell survival in the human neuroblastoma cell line SH-SY5Y. J. Ind. Eng. Chem. 47, 62–73.

Philip, S., Kundu, G.C., 2003. Osteopontin induces nuclear factor κB-mediated promatrix metalloproteinase-2 activation through IκBα/IKK signaling pathways, and curcumin (diferulolylmethane) down-regulates these pathways. J. Biol. Chem. 278, 14487–14497.

Prakash, A., Sharma, S., Ahmad, N., Ghosh, A., Sinha, P., 2011. Synthesis of AgNPs by *Bacillus cereus* bacteria and their antimicrobial potential. J. Biomaterials Nanobiotechnol. 2, 155.

Raffi, M., Hussain, F., Bhatti, T., Akhter, J., Hameed, A., Hasan, M., 2008. Antibacterial characterization of silver nanoparticles against *E. coli* ATCC-15224. J. Mater. Sci. Technol. 24, 192–196.

Rai, M., Ingle, A.P., Gade, A., Duran, N., 2014. Synthesis of silver nanoparticles by *Phoma gardeniae* and *in vitro* evaluation of their efficacy against human disease-causing bacteria and fungi. IET Nanobiotechnol. 9, 71–75.

Rasheed, T., Bilal, M., Iqbal, H.M., Li, C., 2017. Green biosynthesis of silver nanoparticles using leaves extract of *Artemisia vulgaris* and their potential biomedical applications. Colloids Surf. B Biointerfaces 158, 408–415.

Roy, A., Bulut, O., Some, S., Mandal, A.K., Yilmaz, M.D., 2019. Green synthesis of silver nanoparticles: biomolecule-nanoparticle organizations targeting antimicrobial activity. RSC Adv. 9, 2673–2702.

Salem, S.S., Fouda, A., 2020. Green synthesis of metallic nanoparticles and their prosective biotechnological applications: an overview. Biol. Trace Elem. Res.

Salem, S.S., Mohamed, A., El-Gamal, M., Talat, M., Fouda, A., 2019. Biological decolorization and degradation of azo dyes from textile wastewater effluent by *Aspergillus niger*. Egypt. J. Chem. 62, 1799–1813.

Salem, S.S., Fouda, M.M.G., Fouda, A., Awad, M.A., Al-Olayan, E.M., Allam, A.A., et al., 2020. Antibacterial, cytotoxicity and larvicidal activity of green synthesized selenium nanoparticles using *Penicillium corylophilum*. J. Cluster Sci.

Shaheen, T.I., Fouda, A., 2018. Green approach for one-pot synthesis of silver nanorod using cellulose nanocrystal and their cytotoxicity and antibacterial assessment. Int. J. Biol. Macromol. 106, 784–792.

Shaheen, T.I., Salem, S.S., Zaghloul, S., 2019. A new facile strategy for multifunctional textiles development through in situ deposition of SiO2/TiO2 nanosols hybrid. Ind. Eng. Chem. Res. 58, 20203–20212.

Sharaf, O.M., Al-Gamal, M.S., Ibrahim, G.A., Dabiza, N.M., Salem, S.S., El-ssayad, M.F., et al., 2019. Evaluation and characterization of some protective culture metabolites in free and nano-chitosan-loaded forms against common contaminants of Egyptian cheese. Carbohydr. Polym. 223, 115094.

Siddiqi, K.S., Husen, A., Rao, R.A., 2018. A review on biosynthesis of silver nanoparticles and their biocidal properties. J. Nanobiotechnol. 16, 14.

Singh, T., Jyoti, K., Patnaik, A., Singh, A., Chauhan, R., Chandel, S., 2017. Biosynthesis, characterization and antibacterial activity of silver nanoparticles using an endophytic fungal supernatant of *Raphanus sativus*. J. Genet. Eng. Biotechnol. 15, 31–39.

Singh, C., Kumar, J., Kumar, P., Chauhan, B.S., Tiwari, K.N., Mishra, S.K., et al., 2019. Green synthesis of silver nanoparticles using aqueous leaf extract of *Premna integrifolia* (L.) rich in polyphenols and evaluation of their antioxidant, antibacterial and cytotoxic activity. Biotechnol. Biotechnol. Equip. 1–13.

Soliman, A.M., Abdel-Latif, W., Shehata, I.H., Fouda, A., Abdo, A.M., Ahmed, Y.M., 2020. Green approach to overcome the resistance pattern of *Candida* spp. using biosynthesized silver nanoparticles fabricated by *Penicillium chrysogenum* F9. Biol. Trace Elem. Res. (In press).

Sundaravadivelan, C., Nalini, M., 2012. Biolarvicidal effect of phyto-synthesized silver nanoparticles using *Pedilanthus tithymaloides* (L.) Poit stem extract against the dengue vector *Aedes aegypti* L.(Diptera; Culicidae). Asian Pac. J. Trop. Biomed. 1–8.

Taha, Z.K., Hawar, S.N., Sulaiman, G.M., 2019. Extracellular biosynthesis of silver nanoparticles from *Penicillium italicum* and its antioxidant, antimicrobial and cytotoxicity activities. Biotechnol. Lett. 1–16.

Thomas, B., Vithiya, B., Prasad, T., Mohamed, S., Magdalane, C.M., Kaviyarasu, K., et al., 2019. Antioxidant and photocatalytic activity of aqueous leaf extract mediated green synthesis of silver nanoparticles using *Passiflora edulis f. flavicarpa*. J. Nanosci. Nanotechnol. 19, 2640–2648.

Tomaszewska, E., Soliwoda, K., Kadziola, K., Tkacz-Szczesna, B., Celichowski, G., Cichomski, M., et al., 2013. Detection limits of DLS and UV-Vis spectroscopy in characterization of polydisperse nanoparticles colloids. J. Nanomater. 2013, 60.

Valgas, C., Souza, SMd, Smânia, E.F., Smânia Jr., A., 2007. Screening methods to determine antibacterial activity of natural products. Braz. J. Microbiol. 38, 369–380.

Venugopal, K., Rather, H., Rajagopal, K., Shanthi, M., Sheriff, K., Illiyas, M., et al., 2017. Synthesis of silver nanoparticles (Ag NPs) for anticancer activities (MCF 7 breast and A549 lung cell lines) of the crude extract of *Syzygium aromaticum*. J. Photochem. Photobiol. B Biol. 167, 282–289.

Vijaya, J.J., Jayaprakash, N., Kombaiah, K., Kaviyarasu, K., Kennedy, L.J., Ramalingam, R.J., et al., 2017. Bioreduction potentials of dried root of *Zingiber officinale* for a simple green synthesis of silver nanoparticles: antibacterial studies. J. Photochem. Photobiol. B Biol. 177, 62–68.

Vijayabharathi, R., Sathya, A., Gopalakrishnan, S., 2018. Extracellular biosynthesis of silver nanoparticles using *Streptomyces griseoplanus* SAI-25 and its antifungal activity against *Macrophomina phaseolina*, the charcoal rot pathogen of sorghum. Biocataly. Agric. Biotechnol. 14, 166–171.

Vizhi, D.K., Supraja, N., Devipriya, A., Tollamadugu, N.V.K.V.P., Babujanarthanam, R., 2016. Evaluation of antibacterial activity and cytotoxic effects of green AgNPs against Breast Cancer Cells (MCF 7). Adv. Nano Res. 4, 129–143.

Wypij, M., Czarnecka, J., Świecimska, M., Dahm, H., Rai, M., Golinska, P., 2018. Synthesis, characterization and evaluation of antimicrobial and cytotoxic activities of biogenic silver nanoparticles synthesized from *Streptomyces xinghaiensis* OF1 strain. World J. Microbiol. Biotechnol. 34, 23.

Yuan, Y.-G., Zhang, S., Hwang, J.-Y., Kong, I.-K., 2018. Silver nanoparticles potentiates cytotoxicity and apoptotic potential of camptothecin in human cervical cancer cells. Oxid. Med. Cell. Long. 2018.

Yurtluk, T., Akçay, F.A., Avcı, A., 2018. Biosynthesis of silver nanoparticles using novel *Bacillus* sp. SBT8. Prep. Biochem. Biotechnol. 48, 151–159.

Zhang, S., Gao, H., Bao, G., 2015. Physical principles of nanoparticle cellular endocytosis. ACS Nano 9, 8655–8671.